BEAM TESTS OF A PERMANENT MAGNET MEDICAL ACCELERATOR ARC FROM 10–250 MeV*

S. Brooks†, G. Mahler, D. Trbojevic, Brookhaven National Laboratory, Upton, NY, USA

Abstract

The FLASH hadron therapy accelerator proposed by Trbojevic uses permanent magnets with nonlinear fields to allow rapid cycling from 10 to 250 MeV while keeping the ring tune constant. A test beamline of four cells from this ring (22.5 degree angle) was built at BNL and tested at the NSRL facility with protons and at the Tandem Van de Graaff with deuterons. The magnets consist of 24 neodymium-iron-boron (NdFeB) wedges magnetised in different directions and arranged to produce the required nonlinear field profile across the oval aperture for the beam movement, with fields of up to 1.85 Tesla. Beams were transmitted at all rigidities tested over a 5.3× momentum ratio, with output location moving systematically with energy as required.

HADRON THERAPY FACILITY

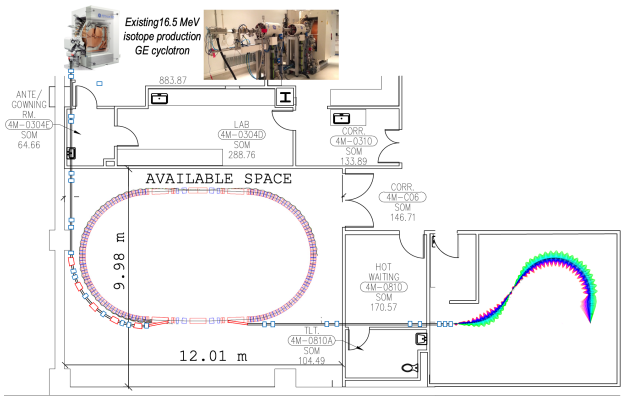

Figure 1: Hadron therapy facility plan view.

A collaboration between BNL and Stony Brook Radiation Oncology has designed a hadron therapy facility capable of ultra-high dose rates (UHDR or FLASH therapy) and rapid energy scanning [1,2]. The facility (Fig. 1) consists of a commercially-available cyclotron injector, followed by a permanent magnet fixed-field accelerator (FFA) ring and a low-dispersion gantry to transport the beam to the patient regardless of the extraction energy.

The wide range of extracted kinetic energies (E_k) shown in Table 1 allows selection of depth within the patient, while the rapid machine cycle rate makes irradiation of the different depths nearly simultaneous. The full treatment charge occurring within a fraction of a second reduces patient motion during the irradiation period and can also provide conditions for the hypothesised FLASH effect that spares healthy tissue.

The optics design of the FFA follows work by Trbojevic who first proposed a non-scaling FFA for medical use [3] and then found adjustments to make the ring tune fixed across the energy range [4]. The team then found systematic ways of generating fixed-tune designs for different applications [5] and better ways of defining the nonlinear magnet fields [6].

Table 1: Hadron Therapy Facility Parameters

Injection E_k	10–30	MeV
Extraction E_k range	65–250	MeV
Arc radius	3.5	m
Machine cycle rate	500–800	Hz
Energy gain per turn	30–45	kV
Treatment charge	60	nC
Treatment time	75–250	ms

FOUR CELL TEST BEAMLINE

A full-scale, full-field prototype of one eighth of the FFA ring arc was built with unit cell given in Table 2. The beamline is four cells long but the cell starts half-way through the F magnet to make the initial and final beam angles zero by symmetry for every energy (Fig. 2).

Table 2: Test Beamline Lattice Cell

Element	**Length (m)**	**Angle (°)**
F	0.18	3.335
O	0.02	0
D	0.123612	2.290
O	0.02	0
Total	0.343612	$5.625 = \frac{360}{64}$
HF	0.09	1.667

Table 3: Orbit Ranges and Peak Fields

Parameter	**F magnet**	**D magnet**	**Unit**
x_{min}	-14.306	-11.148	mm
x_{max}	38.392	24.891	mm
$B_y(0)$	-0.5344	-0.6263	T
$\lvert B_y \rvert_{max}$	1.8462	1.8631	T

The horizontal orbit range and peak fields are given in Table 3. The cell tunes are $Q_x = 0.1608 \pm 0.0004$ and $Q_y = 0.0738 \pm 0.0011$, as plotted in Fig. 3. The beamline before vacuum chamber installation is shown in Fig. 4.

PERMANENT MAGNETS

The field functions of the two magnets are defined by the Fourier coefficients in Table 4 and the formula

$$B_y(x) = c_0 + \sum_{n=1}^{8} s_n \sin(nkx) + c_n \cos(nkx),$$

* Work supported by Brookhaven Science Associates, LLC under Contract No. DE-SC0012704 with the U.S. Department of Energy.

† sbrooks@bnl.gov

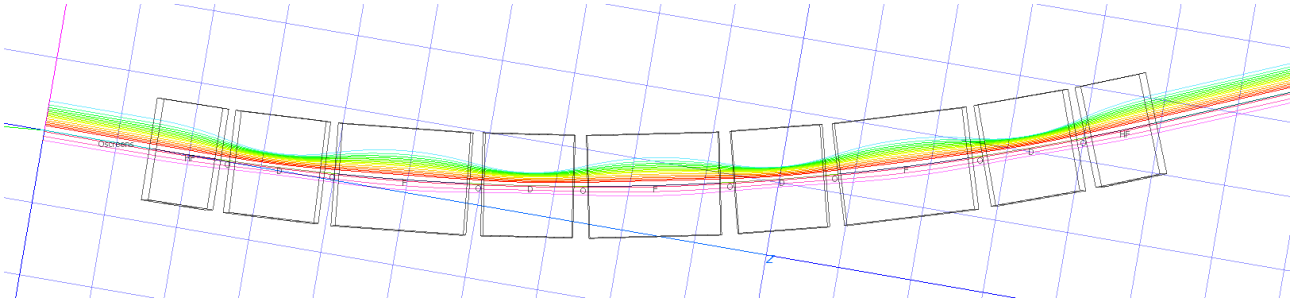

Figure 2: Test beamline simulated orbits from 10 MeV (top, blue) to 250 MeV (bottom, pink). 10 cm grid is shown.

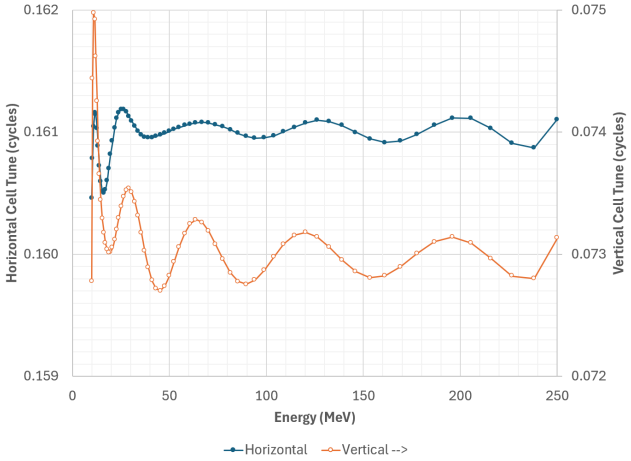

Figure 3: Cell tunes as a function of energy.

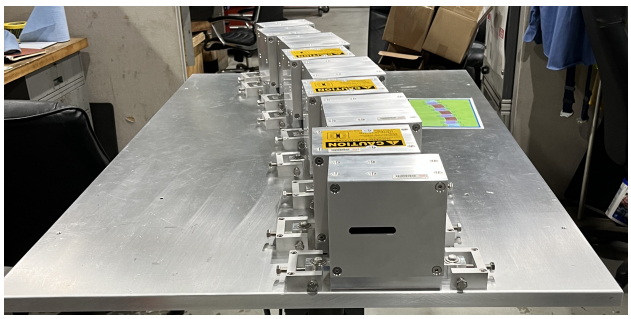

Figure 4: Four cell test beamline.

Table 4: Magnet Fourier Coefficients

	F magnet		D magnet	
n	c_n (T)	s_n (T)	c_n (T)	s_n (T)
0	-0.57736	—	0.88112	—
1	-0.36007	1.85716	-1.72359	-2.55400
2	0.57097	-0.18396	0.19451	0.68841
3	-0.14435	-0.17976	0.02518	-0.22201
4	-0.07936	0.09153	0.01640	0.09403
5	0.07370	0.02026	-0.03576	0.01771
6	-0.01530	-0.03384	0.02866	-0.08665
7	-0.00422	0.01066	-0.01927	0.06162
8	0.00157	-0.00055	0.00641	-0.01511
	k =	60 m^{-1}	k =	60 m^{-1}

where k is a transverse scale factor. Figure 5 shows these functions in the orbit excursion range of each magnet. These values were obtained by computer optimisation of an initial multipole-based MAD design with fields shown in dotted lines.

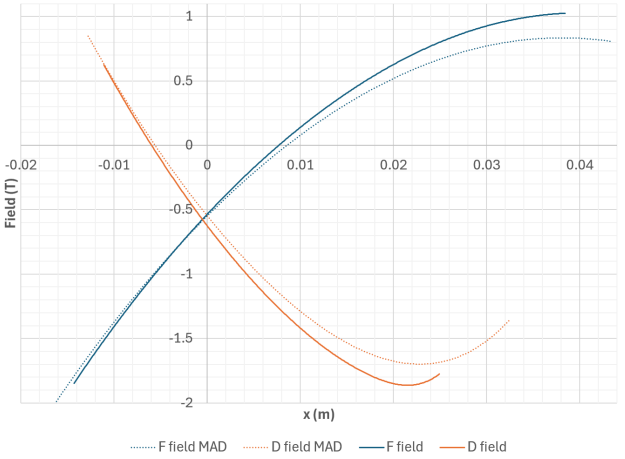

Figure 5: Magnet field functions $B_y(x, 0)$ on the midplane.

Table 5: Magnet Design Parameters

Material	**Grade**	B_r **(T)**
NdFeB	N42EH	1.30
Wedge Type	**Number**	**Angle** (°)
Top/bottom	16	7.5
Left/right	8	30
Parameter	**F magnet**	**D magnet**	**Unit**
x_{GFR}	±26.3	±18.0	mm
Full aperture	64.7 × 12	48.1 × 12	mm
Material area	69.90	93.88	cm^2

Permanent magnets were designed as specified in Table 5 with shapes shown in Fig. 6. This builds on previous work making permanent magnets for the CBETA ERL [7] and then increasing their field to >1.5 Tesla with prototypes for the CEBAF 22 GeV energy upgrade [8, 9].

The magnets were assembled by SABR Enterprises, LLC. in Massachusetts, who specialise in permanent magnet assemblies. The magnets built are shown in Figs. 7 and 8.

Measured Fieldmap

One of the magnets was measured at BNL, giving the fieldmap in Fig. 9, where the three longitudinal segments

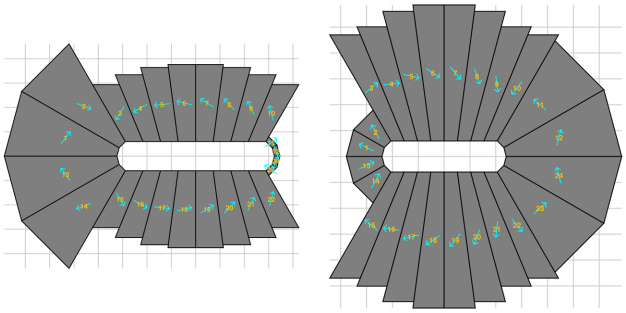

Figure 6: Design cross-sections for F (left) and D (right) magnets. Arrows indicate magnetisation directions. 1 cm grid is shown.

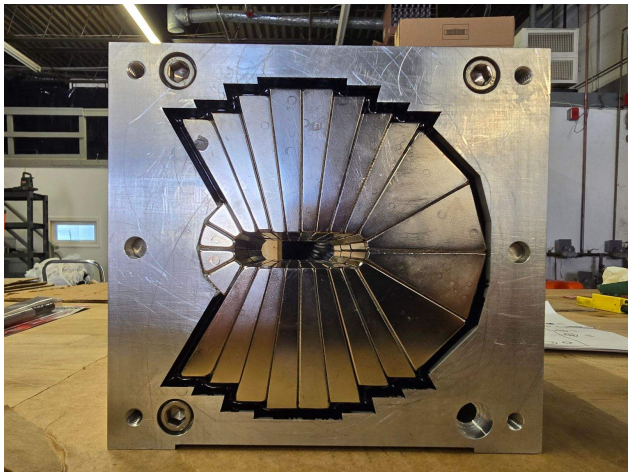

Figure 7: Manufactured D magnet with safety plate removed.

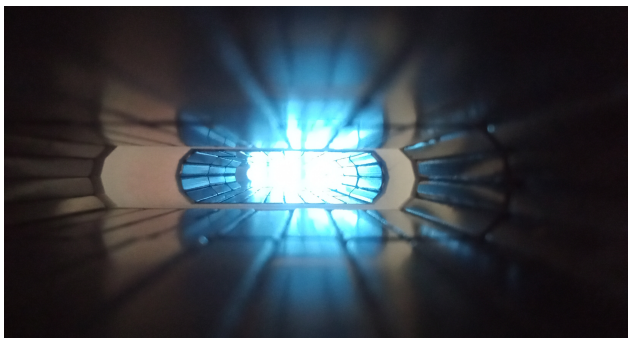

Figure 8: View through beamline magnet apertures.

can be seen. Integrating the field longitudinally allows it to be compared to the nonlinear field function in Fig. 10, showing errors less than 1% of the peak field.

BEAM TRANSMISSION EXPERIMENTS

Two diagnostic plates as shown in Fig. 11 were installed at the entrance and exit of the beamline in Fig. 4 to monitor the beam spot size and position. A pair of screens give some sensitivity to beam angle at the 10 mrad level. The screens retract vertically so that the beam may be intercepted at any of the four locations and the control system was programmed to do this in sequence, synchronised with the RHIC beam pulse.

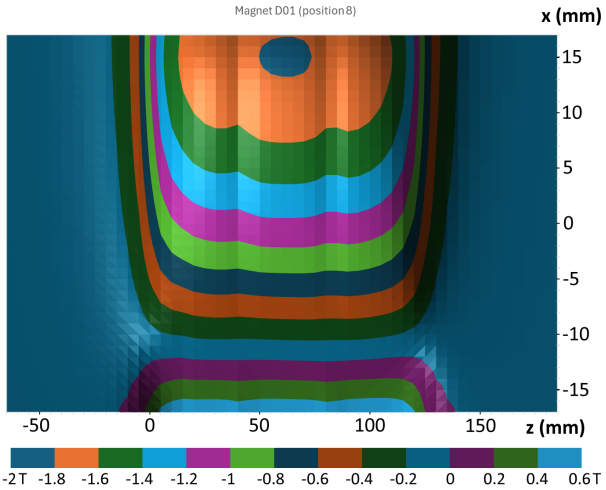

Figure 9: Measured magnet fieldmap $B_y(x, 0, z)$.

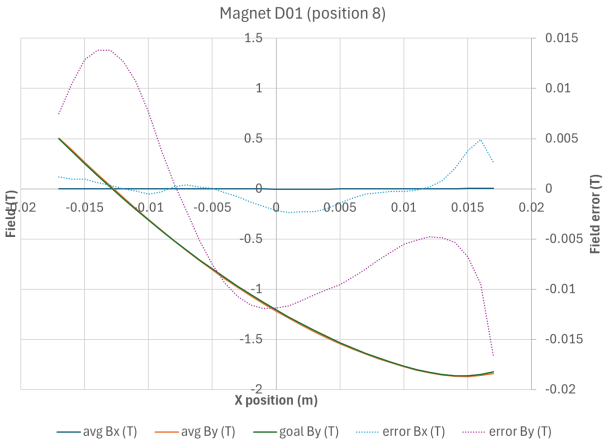

Figure 10: Measured longitudinally-averaged field and error after fitting for Hall probe rotation.

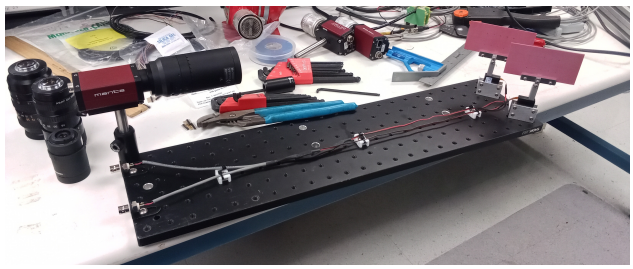

Figure 11: Plate with camera (left) and two fluorescent screens (right), attached to each end of the test beamline.

Table 6: Deuterium Equivalent Energies

Equivalent Proton E_k	**Deuteron E_k (MeV)**
10	12.9
15	14.3
20	16.0
30	20.0
40	24.2
50	28.0

The NASA Space Radiation Facility (NSRL) at BNL provided proton pulses with kinetic energies of 50, 70, 100, 150, 200 and 250 MeV, all of which were transmitted successfully by the beamline. It was difficult to go lower in energy because the RHIC Booster accelerator was not intended for such low energies. The BNL Tandem Van de Graaff can provide protons up to 28.75 MeV but this risked missing intermediate energies where transmission might become difficult: lower rigidity trajectories are more curved and thus more sensitive to errors. A solution was to use deuterium nuclei with the same rigidity as the nominal protons, which gave a higher effective energy range, up to 50 MeV as shown in Table 6. The equivalent energies compensate for both the charge-to-mass ratio of the deuteron and energy loss in the windows and air in front of the beamline's vacuum chamber, which become non-negligible contributions at low energies.

RESULTS

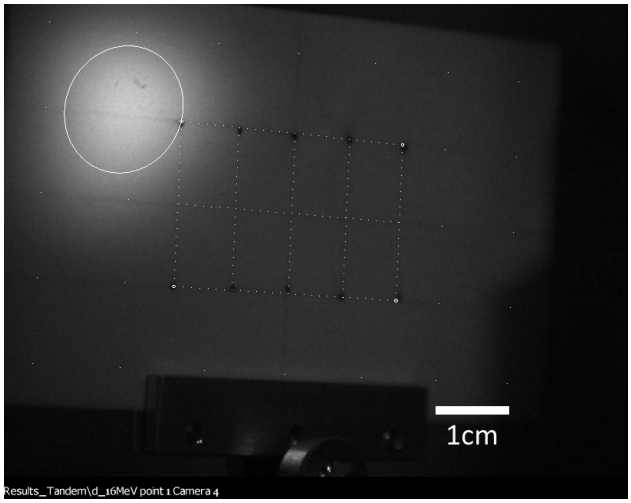

Figure 12: Analysis of single beam spot image with fitted ellipse and calibration points.

Captured images were analysed as shown in Fig. 12, using a 2D Gaussian model with linear background to fit the beam centroid position and 1σ ellipse.

Beam ellipses at all 12 settings (including 50 MeV at both facilities) are shown in Fig. 14, superimposed on their raw camera images. Both the input and output beams move progressively from right to left with decreasing energy, as expected. A small systematic difference in installation height between the two facilities can be seen. The six Tandem input beams on the left also have different shapes, since they come from a linear beamline rather than a ring.

While plotting the centroid positions against energy, more systematic offsets were noticed between the two facilities. This was eventually traced to the diagnostic screens being bolted on differently in the two setups. A re-survey of the screens allowed the results to be corrected as shown in Fig. 15.

The centroids track well with the predicted movement of the closed orbit with energy, although it is also clear the beam was injected 3–8 mm to the high energy side of the desired position. Although the beamline had survey fiducials both inside and outside the vacuum chamber, survey support was not available on the experimental days, so the beamline was aligned with hand-made marks and a laser projected by the facility, which are likely only accurate to a few mm.

The total horizontal tune of the beamline is 0.643, which partly explains why the injection position errors become inverted when looking at the output positions. Other error sources include the large size of the input beam spot in some cases, meaning that the output is scraped by the beamline aperture.

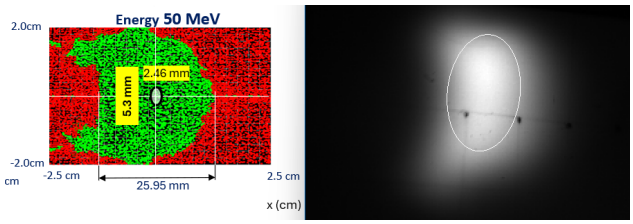

Figure 13: Comparison of computed dynamic aperture shape (left) with observed output beam distribution (right).

Figure 13 shows that the beam scraping effect may be revealing the shape of the dynamic aperture for this nonlinear field lattice, by comparing it with dynamic aperture particle survival in PTC.

Beam input and output angles, which would show as differences between screens 1–2 or 3–4, are zero to within the experimental precision, agreeing with the ideal case.

CONCLUSION AND FUTURE PROSPECTS

The test beamline transmitted beams over the full 10–250 MeV energy range, a factor of 5.3× in momentum. The beam bending angle did not observably differ from the design value of 392.7 mrad (22.5°) for any energy, implying errors below 10 mrad or 2–3%, confirming the multi-energy bend is working consistent with the magnetic field precision. The beam position also tracked in the expected way with energy. This demonstrates engineering feasibility of a non-linear FFA arc with large energy range and high field (1.85 T) permanent magnets. Magnets for the final machine will need to be more accurate but can be fine-tuned by adapting the technique in [7].

Evaluating the tune behaviour will require a better aligned experimental setup, which is planned for a future run. The main modifications planned are:

- Have surveyors inscribe an accurate beamline centre line outside the vacuum chamber, so alignment can be done during experimental runs without survey;
- Add motorised collimator slits in the X and Y axes before the beamline, to reduce the cm-scale 'pencil beam' provided by the facility down to the mm-scale beam needed to avoid scraping.

The collimators will also make it easier to align the beam by centering the X collimator slit on the inscribed centre line, rather than moving the beamline plate or input beam.

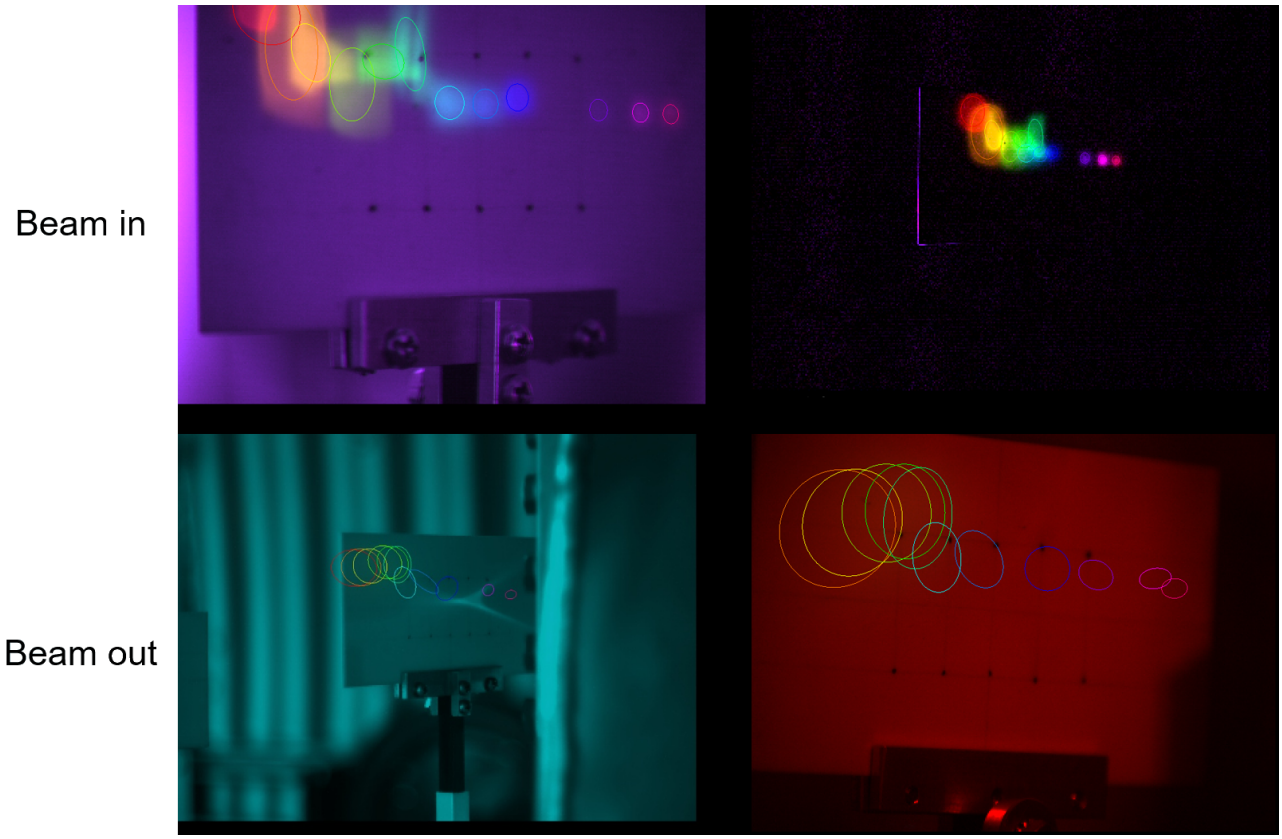

Figure 14: Composite image of all input beam spots and fitted ellipses (top) and output fitted ellipses (bottom) (output beam spots overlap too much to be shown). Red represents 10 MeV equivalent proton E_k and violet 250 MeV.

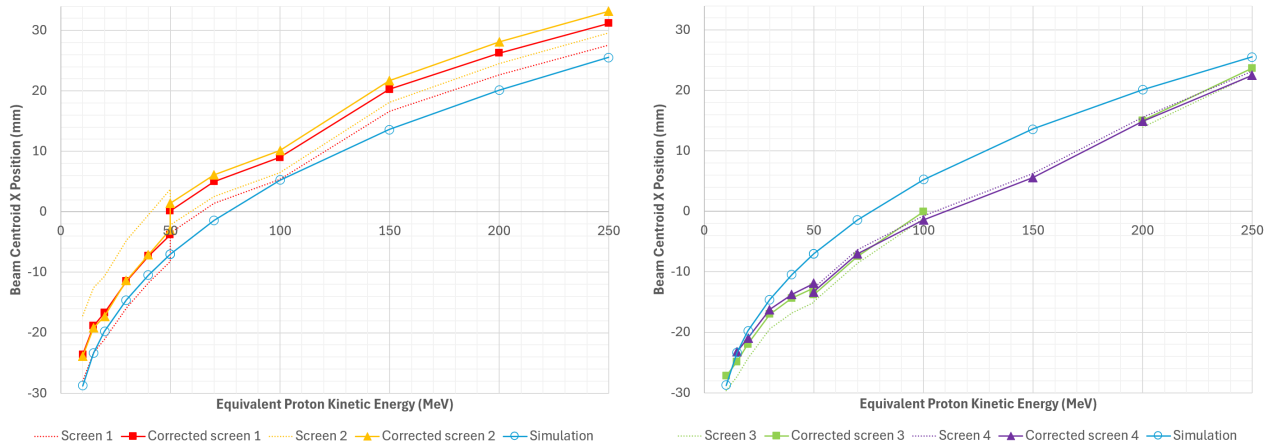

Figure 15: Input (top) and output (bottom) beam centroid x positions, relative to screen centres, as a function of energy.

REFERENCES

[1] X. Qian, D. Trbojevic, S. Brooks, T. Tsang, R. Cattell, J. Kim, T. Zhang and S. Ryu, "Developing Bragg-peak FLASH proton irradiator using permanent magnet synchrotron", *Jour. of Radiosurgery and SBRT* **10**, 123–129 (2026).

[2] D. Trbojevic, G. Mahler and S. Brooks, "FLASH proton therapy facility design with permanent magnet", in *Proc. IPAC'24*, Nashville, TN, May 2024, pp. 3613–3616. doi:10.18429/JACoW-IPAC2024-THPR46

[3] D. Trbojevic, "Non-Scaling Fixed Field Alternating Gradient Permanent Magnet Cancer Therapy Accelerator", United States Patent Application Publication, Pub. No.: US 2014/0252994 A1, Sep. 11, 2014.

[4] D. Trbojevic, J.S. Berg, M. Blaskiewicz and S.J. Brooks, "Fast Cycling FFA Permanent Magnet Synchrotron", in *Proc. IPAC'22*, Bangkok, Thailand, Jun. 2022, pp. 126–129. doi:10.18429/JACoW-IPAC2022-MOPOST029

[5] S. Brooks, "Non-scaling fixed-field proton accelerator with constant tunes", in *Proc. IPAC'23*, Venice, Italy, May 2023, pp. 2257–2260. doi:10.18429/JACoW-IPAC2023-TUPM031

[6] D. Trbojevic, F. Meot, J. Berg and S. Brooks, "Fixed tunes fast cycling permanent magnet proton FFA synchrotron", in *Proc. IPAC'24*, Nashville, TN, May 2024, pp. 467–470. doi:10.18429/JACoW-IPAC2024-MOPR06

[7] S. Brooks, G. Mahler, J. Cintorino, J. Tuozzolo, and R. Michnoff, "Permanent magnets for the return loop of the Cornell-Brookhaven energy recovery linac test accelerator", *Phys. Rev. Accel. Beams* **23**, 112401 (2020). doi:10.1103/PhysRevAccelBeams.23.112401

[8] S. Brooks, "Open-midplane gradient permanent magnet with 1.53 T peak field", in *Proc. IPAC'23*, Venice, Italy, May 2023, pp. 3870–3873. doi:10.18429/JACoW-IPAC2023-WEPM128

[9] S. Brooks and D. Trbojevic, "Optimisation of a permanent magnet multi-energy FFA arc for the CEBAF energy upgrade", in *Proc. IPAC'24*, Nashville, TN, May 2024, pp. 1053–1056. doi:10.18429/JACoW-IPAC2024-TUPC22